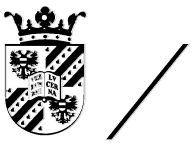

kapteyn astronomical institute

Measuring the CMB with the Kapteyn Radio Telescope

Petar I. Penchev, S4683099, p.i.penchev@student.rug.nl

Abstract: This study aims to measure the Cosmic Microwave Background (CMB) temperature and evaluate atmospheric radio emission using the Kapteyn Radio Telescope, operating in the 10.7–11.7 GHz range. The observations are calibrated using hot and cold loads, allowing precise estimation of system parameters such as gain G_{cal}, receiver noise temperature T_{rec}, and antenna temperature T_{ant}. The CMB temperature was determined to be $T_{cmb} = 3.485 \pm 0.059K$ and $2.272 \pm 0.061K$ from two datasets, with optical depths at zenith $\tau_0 \approx 0.013$ and 0.019 respectively. We fitted a radiative transfer model that accounts for atmospheric attenuation to the data, showing good agreement between theoretical predictions and measurements. The study highlights the challenges posed by atmospheric attenuation and in one of the data sets a satellite interference. Nonetheless we confirmed the effectiveness of the models used and the ability of the telescope to detect the CMB signal. These findings highlight the CMB's importance to cosmology and the importance of precise instrumentation and modeling in radio astronomy.

1 Introduction

The Cosmic Microwave Background (CMB) is radiation emitted approximately 380,000 years after the Big Bang, when protons and electrons combined to form neutral hydrogen; this epoch is known in cosmology as recombination. This event allowed photons to decouple from matter and propagate freely through space, creating a nearly uniform radiation field. This makes the CMB a cornerstone of modern cosmology, offering profound insights into the origins, structure, and evolution of the early universe [Ryden (2017)].

The key observational characteristics of the CMB include its blackbody spectrum with a peak at a temperature of approximately $2.725K$ and its slight anisotropies (temperature fluctuations) at the microkelvin level. These anisotropies, first detected by the Cosmic Background Explorer (COBE) satellite in 1992, encode information about the initial density perturbations that eventually led to the large-scale structures we observe today [Team (1992)]. Subsequent missions such as the Wilkinson Microwave Anisotropy Probe (WMAP) and the Planck satellite have significantly improved those measurements, the latter being the most precise measurements we have [Collaboration (2018)].

Historically, the discovery of the CMB by [Penzias and Wilson (1965)] marked a paradigm shift in cosmology, which made the hot Big Bang theory the only sensible explanation of the origin of the universe. This finding were theorised earlier in the late 1940s by Alpher, Herman, and Gamow who showed that the universe had to be hot and dense during its early stages for the Big Band theory to be consistent [Alpher and Herman (1948)].

The CMB has helped cosmologists finetune their models pertaining to dark energy, dark matter, inflation, determining the gemotry of the universe, and many more. It also enables precise measurements of critical parameters, such as the Hubble constant and the age of the universe. The importance of the CMB cannot be overstated [Collaboration (2018)].

This experiment aims to measure the temperature of the CMB and test our atmospheric emission and attenuation models, using the Kapteyn Radio Telscope (more about this telescope in Section 3). We observed in the narrow range of $10.7GHz$ to $11.7GHz$, which helps us to have a low value for the optical depth and low attenuation.

2 Theory

2.1 Range of observation

The CMB radiation follows the Planck's function of a black-body. This curve along with the observing band of the Kapteyn Radio Telescope is shown in Figure 2.1.

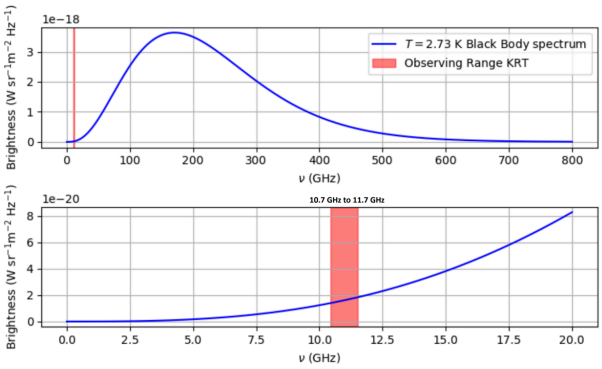

Figure 2.1: The figure on the top represents the blackbody spectrum of an object with a temperature equal to $2.73K$ (which is the aggreed upon value of the CMB [Collaboration (2018)]). The figure on the bottom shows a zoomed in version of the spectrum with the observing band of the KRT in red. [Formsma (2017)]

Obviously it is not very efficient to observe at such a low intensity and it would make much more sense to observe at a higher frequencies, lets say $175GHz$ instead, as this is the peak of the distribution. The problem with that becomes evident in Figure 2.2

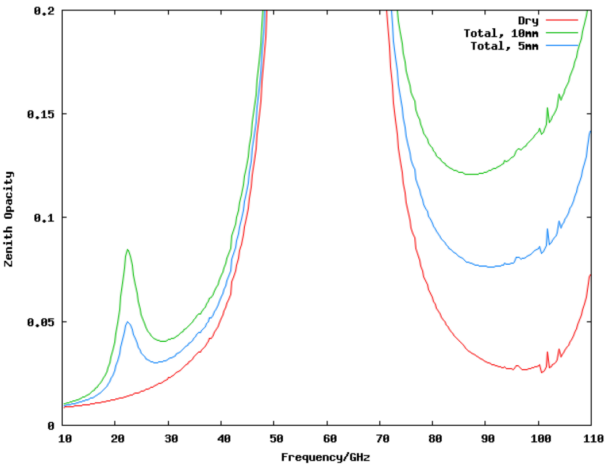

Figure 2.2: The figure represents the different values for the zenith opacity in terms of frequency. There are three atmospheric conditions present, dry (red), 5mm precipitable water vapor (blue), and with 10mm (green). [Formsma (2017)]

The absorption from the various elements in our atmoshpere (mainly water vapor H_20 and oxygen 0_2) cause attenuation. This attenuation however is quite week around the $10.7 - 11.7GHz$ range, with a value of around $\tau_0 \approx 0.01$, where τ_0 is the zenith opacity (more about opacity in Section 2.2). This is the reason why the KRT was design to observe at that range [Formsma (2017)].

2.2 Opacity [Formsma (2017)]

Our CMB signal changes because it passes through the atmosphere. This is due to various effects, such as absorption, emission, reflection, and scattering. The measure of how much the electromagnetic radiation gets attenuated is called the opacity. The amount of attenuation also depends on the optical depth of the medium and the path-length that lights has to travel. Assuming that the atmosphere can be approximated as a slab on top of the surface of the Earth we can make the assumption that the path length can be related by the path at zenith and the zenith angle z described by the following equation,

$$\tau(z) = \tau_0 \cdot X(z,t). \tag{2.1}$$

where τ_0 is the optical depth at zenith, and $X(z,t)$ is the time dependent air mass in terms of zenith angle. Assuming that the atmospheric optical depth is constant duiring obsevation [Sweijen (2015)], Equation 2.1 can be simplified to

$$\tau(z) = \frac{\tau_0}{\cos(z)} \tag{2.2}$$

2.3 Radiative Transfer [Formsma (2017)]

Now that we understand how the opacity of a medium is releated to the path length, we can determine the influence of the medium on our observations. We ca describe this change using the equation of radiative transfer,

$$\frac{dI_\nu}{ds} = -\kappa_\nu I_\nu + \epsilon_\nu, \tag{2.3}$$

where κ_ν is the linear absorption coefficient, and ϵ_ν is the emission coefficient [Chandrasekhar (1960)].

Using Kirchhoff's Law for (which also holds in Local Thermodynamic Equilibrium) we can rewrite Equation 2.3 as

$$-\frac{1}{\kappa_\nu}\frac{dI_\nu}{ds} = I_\nu - B_\nu(T). \tag{2.4}$$

Solving for the intesity along a path of length s and assuming an isothermal medium [Formsma (2017)] we are left with

$$I_\nu(s) = I_\nu(0)e^{-\tau_\nu} + B_\nu(T)\left(1 - e^{-\tau_\nu}\right). \tag{2.5}$$

2.4 Deriving the antenna temperature

Using the the Rayleigh-Jeans approximation for a small wavelength ($h\nu \ll kT$) (Wilson et al., 2013) the Planck's Law simplifies to

$$B_\nu(T) = \frac{2\nu^3}{c^2}\frac{1}{e^{h\nu/kT}-1} \approx \frac{2\nu^2}{c^2}k_B T \qquad (2.6)$$

Using the proportionality between the brightness B_ν and the temperature T of the source we can express the brightness of an extended object as its brightness temperature T_b given by,

$$T_b = \frac{c^2}{2k_B\nu^2}I_\nu. \qquad (2.7)$$

where I_ν is the specific intensity of the radiation.

For an isothermal medium, the brightness temperature of both the atmosphere and the CMB can be substituted into the radiative transfer equation, giving us

$$T_{ant}(s) = T_{cmb}e^{-\tau_\nu(s)} + T_{atm}\left(1 - e^{-\tau_\nu(s)}\right), \qquad (2.8)$$

where $T_{atm} = 275 \pm 0.5K$ is the temperature of the atmosphere at the day of observation, T_{cmb} is the temperature of the CMB, $T_{ant}(s)$ is the temperature of the antenna temperature, and $\tau_\nu(s)$ is the optical depth in terms of path length.

From Section 2.2 we know that the optical depth is also given by Equation 2.2 which allows us to do the following substitution,

$$T_{ant}(z) = T_{cmb}e^{-\tau_0/\cos(z)} + T_{atm}\left(1 - e^{-\tau_0/\cos(z)}\right), \qquad (2.9)$$

which gives us the antenna temperature in terms of a zenith angle.

2.5 Accounting for amplifier gain

We know from [Mulder (2015)] that the output of the telescope is not only that of the observed source, it also adds its own signal to what it measures. This is described as the receiver noise, which can be expressed as an equivalent noise temperature. This means that the total output of the system is equal to the signal from the source plus the receiver temperature, and is given by,

$$T_{sys} = T_{ant} + T_{rec}, \qquad (2.10)$$

where T_{rec} is the noise temperature from the telescope, and T_{sys} is the system temperature. However in order to measure the signal we need to first amplify it, as the signal is too weak, meaning that the measured power is releated to the system temperature in the following way

$$P_{out}[W] = T_{sys}G_{cal}, \qquad (2.11)$$

where $P_{out}[W]$ is the measured power in watts, and G_{cal} is the calibration constant for the observation [Formsma (2017)]. The calibraion is given by

$$G_{cal} = \frac{P_H - P_C}{T_H - T_C}, \qquad (2.12)$$

where P_H and P_C are the power measured by the telescope facing the hot and cold load with temperatures T_H and T_C respectively.

More about the way we derive the reviever temperature T_{rec}, and the two loads in Section 3.

3 Observations [Formsma (2017)]

The Kapteyn Radio Telescope (KRT) observes the CMB at 11 GHz. Four astronomy bachelor students built it in 2015 as part of their project.

The telescope features a horn antenna, two amplifiers, and a bandpass filter as its front end. A local oscillator and mixer down-convert the signal to a more manageable frequency. The system mounts on an aluminum frame, with a stepper motor enabling precise movement along the zenith. Bram Lap designed the horn antenna, which is a Picket-Potter type, known for its low side lobes and a full-width half maximum of 15° of the sky.

The telescope operates via a Raspberry Pi-based system for control [Sweijen (2015)]. To calibrate observations, we must determine the receiver temperature T_{rec}. We achieve this using the y-factor method (more details can be found on page 9 of [Formsma (2017)]), which provides the following expression for the receiver temperature:

$$T_{rec} = \frac{T_H + yT_C}{y - 1}. \qquad (3.1)$$

Here, T_H, the hot load, equals $275 \pm 0.5\,K$, and T_C, the cold load cooled by liquid nitrogen, is $77.36\,K$. We performed this calibration before the observation, ensuring the telescope's measurements remain accurate and compensate for any system drift.

During the observation, we rotate the horn antenna to view these loads and then proceed with the sky observation, making 24 observations every 5° starting from 60° and ending at 175°, ensuring precise and reliable sky measurements.

4 Results

4.1 Measuring the CMB temperature from the 5.data155637_cmb dataset [Table A.1]

Preproccessing the data

Firstly in order to do our analysis we need to transform the powers given in dBm to Watts. We know

that the conversion is done thourgh the following relation,

$$P[W] = 10^{-3} W 10^{(P[dBm]/10)} \tag{4.1}$$

where the symbols have their usual meaning.

We also need to discard the first and last two data-points as they correspond to the measurment of the hot and cold load at the beginning and the end of the observation [Formsma (2017)]. After this our data is ready and can be seen in Figure 4.1 below.

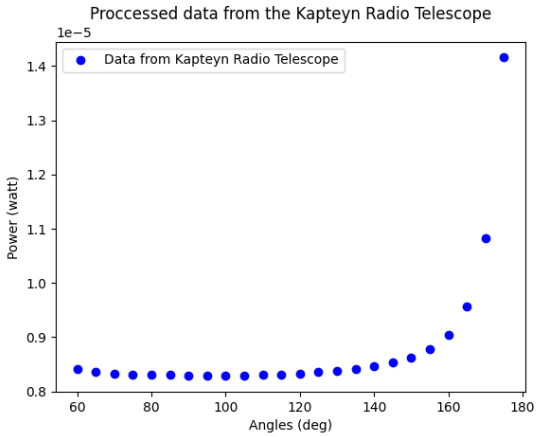

Figure 4.1: The figure represents a plot of the raw data where the x-axis represents the angles of observation in degrees and on the y-axis is the measured power in watts. This dataset can be found in Table A.1.

Finding the antena temperatures

The first and last two measurements are used to find the calibration constant. We use the result of Equation 2.12, and the temperatures of the hot and cold load, as recorded by [Formsma (2017)], namely $T_H = 275 \pm 0.5K$ and $T_C = 77.36 \pm 0.01K$ we found that,

$$G_{cal} = 9.039 \pm 0.023 \times 10^{-8} \frac{W}{K}. \tag{4.2}$$

in watt per kelvin. The error in the estimate has been propagated with the formula given in Equation B.2.

Using the hot and cold load once more, and the result in Section 3, particularly Equation 3.1 we get a reciever temperature of

$$T_{rec} = 84.660 \pm 0.410K. \tag{4.3}$$

Now that we have found G_{cal} we are fully equipped with everything we need in order to find the system temperature. Turning our attention to Equation 2.11 and solving for T_sys we get

$$T_{sys} = \frac{P_{out}[W]}{G_{cal}}, \tag{4.4}$$

where the error is given by Equation B.3. Removing the reciever temperature from the system temperature gives us the antena temperature,

$$T_{ant} = T_{sys} - T_{rec} \tag{4.5}$$

with its appropriate error given in Equation B.4. A graph with the antenna temperature in terms of the angle of observation is shown in the figure bellow.

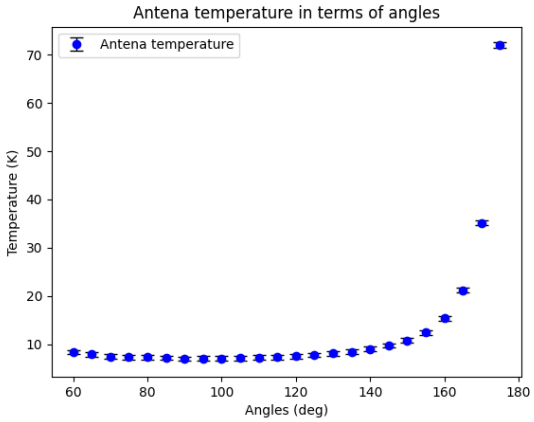

Figure 4.2: The figure represents a plot of the antena temperature against the angles of observation in degrees. The x-axis represents the angles in deg and the y-axis is the temperature in Kelvin.

Finding the CMB temperature

In order to find the CMB temperature we need to fit the antena model described in Section 2.4, Equation 2.9. However, the problem is that the last few data points are heavily dominated by the attenuation of the atmosphere and have quite a high temperature as can be seen in Figure 2.9. This is the case due to observing at an angle very close to the horizon and looking through a lot more atmosphere. Looking at a zenith angle of $z = 80\,\text{deg}$ we know that we are looking through about an airmass of 5.5 Young (1994). Since we are trying to minimize the effect of all of this airmass we are discarding some of the data points from our analysis. The discarded graph can be seen in Figure 4.4.

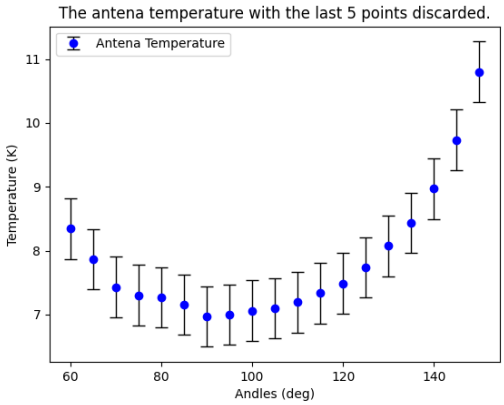

Figure 4.3: The figure represents a plot of the antena temperature against the angles of observation in degrees with the last 5 points discarded due to too much contribution from the atmosphere. The x-axis represents the angles in deg and the y-axis is the temperature in Kelvin.

Now we can fit the model to our data points and we get a value for the CMB equal to,

$$T_{cmb} = 3.485 \pm 0.059K, \tag{4.6}$$

as well as an optical depth at zenith equal to,

$$\tau_0 = 0.013 \pm (0.005 \times 10^{-4}) \tag{4.7}$$

The fitted model with the aforementioned values can be seen in the figure bellow.

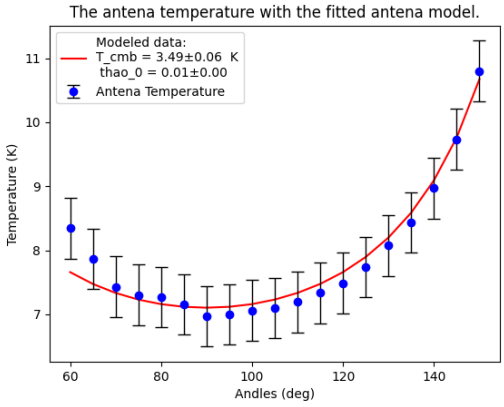

Figure 4.4: The figure represents a plot of the antena temperature against the angles of observation along with the fitted anena model in red. The x-axis represents the angles in deg and the y-axis is the temperature in Kelvin.

Summary of the results

Parameter	Value
G_{cal}	$9.039 \pm 0.229 \times 10^{-8} \frac{W}{K}$
T_{rec}	$84.660 \pm 0.410K$
T_{cmb}	$3.485 \pm 0.059K$
τ_0	$0.013 \pm (0.005 \times 10^{-4})$

Table 4.1: Summary of the relevant parameters and their uncertainties.

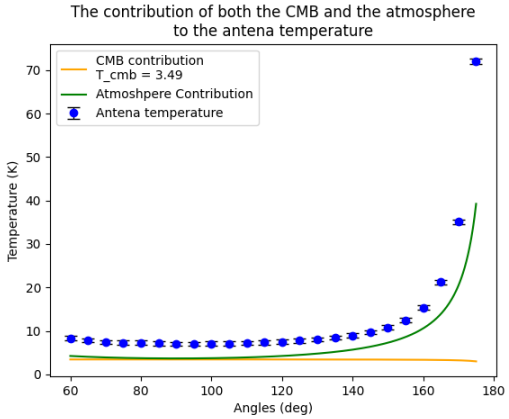

Figure 4.5: The figure represents the contribution from both the cmb (in orange) and the atmosphere (in green) to the antena temperature. The x-axis represents the angles in deg and the y-axis is the temperature in Kelvin.

4.2 Measuring the CMB temperature from the 12.data160408_cmb dataset [Table A.2]

Preproccessing the data

Following the same procedure as in Section 4.2 we get the following plot of the data:

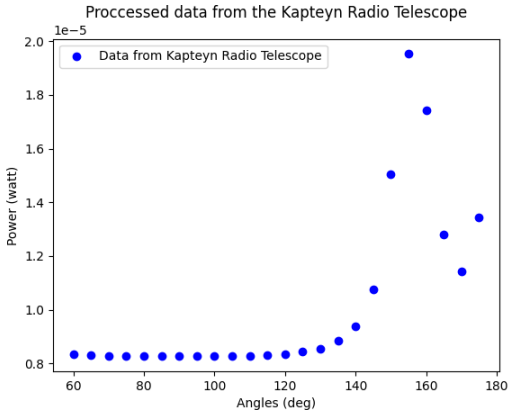

Figure 4.6: The figure represents a plot of the raw data where the x-axis represents the angles of observation in degrees and on the y-axis is the measured power in watts. This dataset can be found in Table A.2.

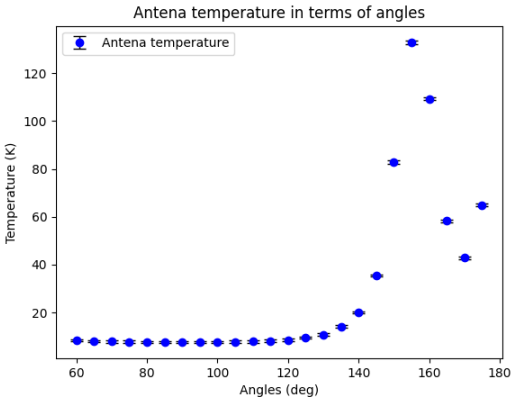

Figure 4.7: The figure represents a plot of the antena temperature against the angles of observation, with the suspected satellite passing. The x-axis represents the angles in deg and the y-axis is the temperature in Kelvin.

It is evident by comparing Figure 4.6 and Figure 4.1 that there is a contribution in the former from something Gaussian in nature. One possible explanation for this as pointed out by [Formsma (2017)] can be a geo-stationary satellites. They reside in the far field of the horn antenna, causing a point source response. This looks like a Gaussian peak in the data, exactly what we see.

Finding the antena temperatures

Again following the same procedure as in Section 4.2 we found a calibration constant of,

$$G_{cal} = 8.981 \pm 0.023 \times 10^{-8} \frac{W}{K}, \qquad (4.8)$$

and a receiver temperature of,

$$T_{rec} = 84.550 \pm 0.410 K. \qquad (4.9)$$

Which are similar to the ones found with the other dataset, which is to be expected, since we are measuring with the same telescope. These two as described in Section 2.4 gives us the ability to find the antena temperature, whose plot can be seen bellow.

Getting rid of the satellite contribution

We know that the satellite can be modeled as a Gaussian, so what we did was try to fit a Gaussian to our data. We got rid of the last data point, as this is not part of the gaussian profile, but rather from the atmoshpere. We use the curve_fit() function from the scipy.optimize module [Jones et al. (01)] and were able to fit the Gaussian to the data. This can be seen in Figure 4.8.

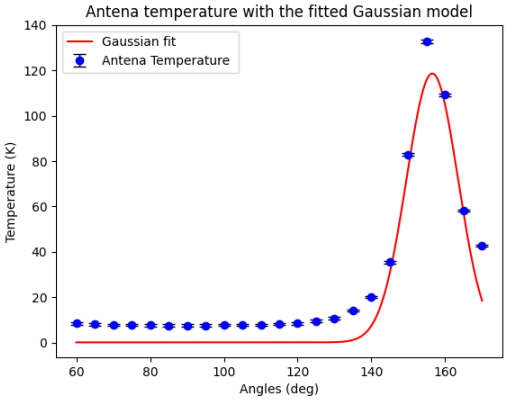

Figure 4.8: The figure represents a plot of the antena temperature along with the Gaussian fit used to model the satellite. The x-axis represents the angles in deg and the y-axis is the temperature in Kelvin.

An import quantity we can find from this fit it is Full-width at Half Maximum (FWHM). Since the satellite is effectively a point source, as it lies in the far field, the FWHM tells us about the angular width of the main lobe. This determines the telescope's ability to resolve fine details in the

sky. It also defines the Field of View (FOV) of the KRT. We found a value for the FWHM equal to,

$$FWHM = 16.517^{\circ} \pm 0.555 \times 10^{-04} \qquad (4.10)$$

The FWHM can be seen in the Figure 4.9.

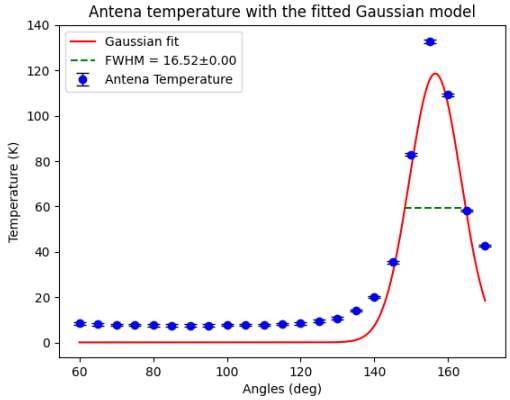

Figure 4.9: The figure represents a plot of the antena temperature along with the Gaussian fit and its Full-Width at Half Maximum (FWHM). The x-axis represents the angles in deg and the y-axis is the temperature in Kelvin.

Now that we have a model for the satellite we can remove its contribution from the antena temperature in Figure 4.7. The resulted antena temperaures can be seen in Figure 4.10.

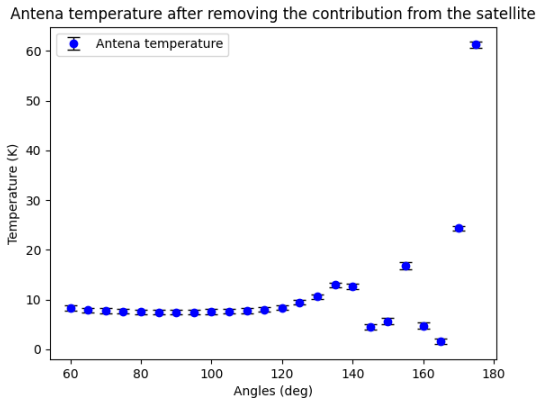

Figure 4.10: The figure represents a plot of the antena temperature without the contribution of the satellite. The x-axis represents the angles in deg and the y-axis is the temperature in Kelvin.

Finding the CMB temperature

We remove the last few points. The antena temperature with the last 12 points discarded can be seen in Figure 4.11.

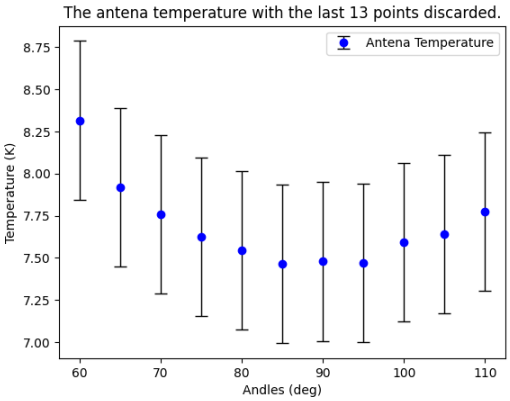

Figure 4.11: The figure represents a plot of the antena temperature without the last 13 points. The x-axis represents the angles in deg and the y-axis is the temperature in Kelvin.

Now we use the findings in Section 2.4, Equation 2.9 to model the contributions from the CMB and the atmosphere. The fitted antena model is shown in Figure 4.12

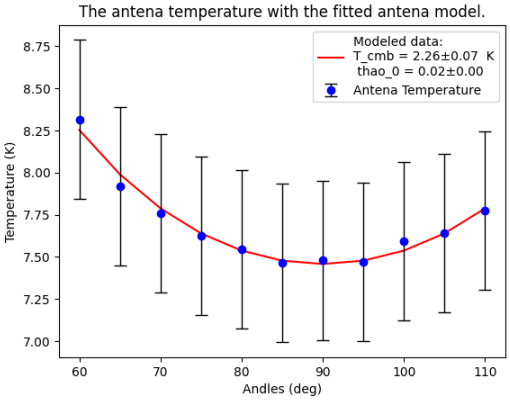

Figure 4.12: The figure represents a plot of the antena temperature alongside the fitted antena model for a CMB temperature of $2.26 \pm 0.07K$ and an optical depth 0.02. The x-axis represents the angles in deg and the y-axis is the temperature in Kelvin.

From the fitted model we infer that the temperature of the CMB is equal to,

$$T_{cmb} = 2.272 \pm 0.061K. \qquad (4.11)$$

The optical depth at zenith is equal to,

$$\tau_0 = 0.019 \pm (0.741 \times 10^{-7}) \qquad (4.12)$$

Summary of the results

Parameter	Value
G_{cal}	$8.981 \pm 0.023 \times 10^{-8} \frac{W}{K}$
T_{rec}	$84.550 \pm 0.410 K$
T_{cmb}	$2.272 \pm 0.061 K$
τ_0	$0.019 \pm (0.741 \times 10^{-7})$

Table 4.2: Summary of the relevant parameters and their uncertainties.

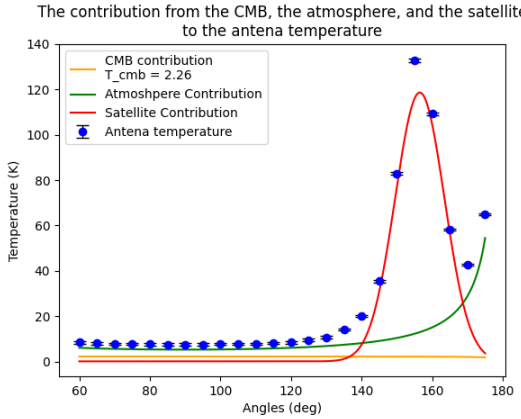

Figure 4.13: The figure represents the contribution from both the cmb (in orange), the atmosphere (in green), and the satellite to the antena temperature. The x-axis represents the angles in deg and the y-axis is the temperature in Kelvin.

5 Discussion

The findings of a low CMB temperature in both data sets combined with the fact that the universe is expanding [Hubble (1929)], tells us that the universe had a very hot and dense beginning. This insight points to the well established Big Bang theory as the most probable explanation of the evolution of our universe. Moreover the anisotropy in this radiation can tell us a lot about the large scale structures we see today as shown in [Collaboration (2018)]. The small gain that our system has makes it very difficult to detect those small anisotropies and are outside of the scope of this paper. However the wide field of view of the telescope, covering a wide area of the sky, makes the telescope ideal for capturing the temperature of the CMB.

The low optical depth also indicates minimal absorption and emission caused by atmospheric attenuation in the observed frequency range, as shown by theory (see Figure 2.2). This suggest minimal interference from the atmosphere, meaning that its effect on the measurements of the CMB is small.

The experimentally derived values for T_{cmb} align reasonably well with the established value of 2.725 K [Collaboration (2018)]. We confirmed the effectiveness of the atmospheric emission model in predicted the observed attenuation as well as the radiative transfer equation, modified for opacity in terms of zenith angle. These models approximated the antena temperature quite well, which supports the validity of the theoretical framework. The Raylegh-Jeans approximation, and the Planck's Law, also proved to hold and were in agreement between measurement and theory.

6 Conclusion

The experiment successfully determined a CMB temperature of $T_{cmb} = 3.485 \pm 0.059$ K in the first dataset and $T_{cmb} = 2.272 \pm 0.061$ K in the second, with optical depths $\tau_0 = 0.013 \pm (0.005 \times 10^{-4})$ and $\tau_0 = 0.019 \pm (0.741 \times 10^{-7})$, respectively.

The slight discrepancies highlight sensitivity to atmospheric contributions at different zenith angle observations, and the effect of the assumptions that the atmospheric optical depth is constant during observation (see Section 2.2). We also found that contributions from atmospheric attenuation were dominant at lower angles due to increased air mass and had to discard those measurements.

The radiometers of the KRT are characterized by a gain (G_{cal}) ranging from $8.981 \pm 0.023 \times 10^{-8}$ W/K to $9.039 \pm 0.023 \times 10^{-8}$ W/K. We determined the effective area, by examining the FWHM of the Gaussian profile (caused by a satellite passing), to be $16.517^\circ \pm 0.555 \times 10^{-04}$, which is also our FOV.

Incorporating hot and cold loads in the calibration, allowed us to measure preciesly the receiver temperature (T_{rec}) at approximately 84.660 ± 0.410 K accross both observations.

The experiment could be improved by trying to capture more objects in the far field, to better determine the FWHM. Measurements over different days would also be helpful in modeling the changes in the atmosphere better.

References

Alpher, R. A. and Herman, R. C. (1948). Evolution of the universe. *Nature*, 162:774–775.

Chandrasekhar, S. (1960). *Radiative Transfer*. Dover Publications, New York. A foundational work discussing the principles of radiative transfer and its applications.

Collaboration, P. (2018). Planck 2018 results. vi. cosmological parameters. *Astronomy & Astrophysics*, 641:A6.

Formsma, J. (2017). *Job Formsma Thesis Final*. PhD thesis, University of Groningen. Accessed: 2024-12-29.

Hubble, E. (1929). A relation between distance and radial velocity among extra-galactic nebulae. *Proceedings of the National Academy of Sciences of the United States of America*, 15(3):168–173.

Jones, E., Oliphant, T., Peterson, P., et al. (2001–). SciPy: Open source scientific tools for Python.

Mulder, W. (2015). Calibration of a 11 ghz pickett-potter horn and measurements of the cosmic microwave background. Bachelor thesis, University of Groningen.

Penzias, A. A. and Wilson, R. W. (1965). A measurement of excess antenna temperature at 4080 mc/s. *The Astrophysical Journal*, 142:419–421.

Ryden, B. (2017). *Introduction to Cosmology*. Cambridge University Press, Cambridge, UK, 2nd edition.

Sweijen, F. (2015). Computer control of a horn antenna and measuring the sun at 11 ghz. Technical report, Your Institution Name.

Team, C. (1992). Structure in the cobe differential microwave radiometer first-year maps. *The Astrophysical Journal Letters*, 396:L1–L4.

Wilson, T. L., Rohlfs, K., and Hüttemeister, S. (2013). *Tools of Radio Astronomy*. Springer, Berlin, Heidelberg, 6th edition. Comprehensive reference for the fundamentals of radio astronomy.

Young, A. T. (1994). Air mass and refraction. *Applied Optics*, 33(6):1108–1110.

A Appendix

Code

All the code used to preprocess the data and estimate the relevant temperatures is available here and is allowed to be viewed duiring grading this report:
https://github.com/Aureusa/Measuring-the-CMB-with-the-Kapteyn-Radio-Telescope

Datasets used in this report

Angle (deg)	Power (dBm)
-88	-18.3463087
0	-14.8813624
60	-20.753559
65	-20.7758651
70	-20.7965149
75	-20.8024792
80	-20.8039634
85	-20.809645
90	-20.8184754
95	-20.8168796
100	-20.8139596
105	-20.8121908
110	-20.8078214
115	-20.8011065
120	-20.7937533
125	-20.7819828
130	-20.7663205
135	-20.7494584
140	-20.7245282
145	-20.6892057
150	-20.6405242
155	-20.5668301
160	-20.4393164
165	-20.1915182
170	-19.6544986
175	-18.4896901
0	-14.8780523
-88	-18.3395781

Table A.1: Angle and Power Data without satellite (5.data155637_cmb).

Angle (deg)	Power (dBm)
-88	-18.3766911
0	-14.9091866
60	-20.7850606
65	-20.8036009
70	-20.8111106
75	-20.8173792
80	-20.8211991
85	-20.8250181
90	-20.8243143
95	-20.8247336
100	-20.8189881
105	-20.816621
110	-20.8104203
115	-20.7993086
120	-20.7825656
125	-20.7317004
130	-20.6759704
135	-20.5269383
140	-20.2702488
145	-19.6759025
150	-18.2289233
155	-17.0952106
160	-17.5911683
165	-18.9210877
170	-19.4174681
175	-18.7212826
0	-14.9091022
-88	-18.37131

Table A.2: Angle and Power Data with satelite (12.data160408_cmb).

B Appendix

Error propagation

The error in the receiver temperature:

$$\sigma_{T_{rec}} = \sqrt{\left(\frac{1}{y-1}\sigma_{T_H}\right)^2 + \left(\frac{y}{y-1}\sigma_{T_C}\right)^2 + \left(\frac{-(T_H + yT_C)}{(y-1)^2}\sigma_y\right)^2} \tag{B.1}$$

The error in the calibration:

$$c \tag{B.2}$$

The error in the system temperature:

$$\sigma_{T_{sys}} = \frac{P}{G_{cal}}\sqrt{\left(\frac{\sigma_P}{P}\right)^2 + \left(\frac{\sigma_{G_{cal}}}{G_{cal}}\right)^2} \tag{B.3}$$

The error in the antena temperature:

$$\sigma_{T_{ant}} = \sqrt{\sigma^2_{T_{sys}} + \sigma^2_{T_{rec}}} \tag{B.4}$$

The error in the CMB temperature:

$$\begin{aligned}\sigma_{T_{cmb}} = &\sqrt{\left(\frac{-\left(1 - e^{-\tau_0/\cos(z)}\right)}{e^{-\tau_0/\cos(z)}}\sigma_{T_{atm}}\right)^2 + \right.\\ &\left(\frac{1}{e^{-\tau_0/\cos(z)}}\sigma_{T_{sys}}\right)^2 +\\ &\left(\frac{-1}{e^{-\tau_0/\cos(z)}}\sigma_{T_{rec}}\right)^2 +\\ &\left(\frac{T_{atm}\cdot e^{-\tau_0/\cos(z)}\left(1 - e^{-\tau_0/\cos(z)}\right)}{\cos(z)\cdot e^{-\tau_0/\cos(z)}}\sigma_{\tau_0}\right)^2 +\\ &\left.\left(\frac{T_{atm}\left(1 - e^{-\tau_0/\cos(z)}\right)\cdot\frac{\tau_0\sin(z)}{\cos^2(z)}}{e^{-\tau_0/\cos(z)}}\sigma_z\right)^2\right.\end{aligned}$$